Levels of ^{105}Pd populated in the decay of ^{105}Ag^{m,g} and comparison with interacting boson-fermion model calculations

R. A. Meyer
Montgomery College, Takoma Park, Maryland 20850

S. V. Jackson
First Presbyterian Church, Lebanon, Oregon 97355

S. Brant and V. Paar
Department of Physics, Faculty of Science, University of Zagreb, 10000 Zagreb, Croatia
(Received 6 February 1995; revised manuscript received 25 June 1996)

Deexcitation properties of low-spin levels in ^{105}Pd populated in the decay of ^{105}Ag^m and ^{105}Ag^g are investigated. The calculation for ^{105}Pd is performed in the interacting boson-fermion model (IBFM), using a nearly spherical boson core corresponding to ^{104}Pd. As a result, we obtain an approximate quasiweak-coupling pattern, which is in contrast to previously assumed symmetric rotor model calculations. Rather good agreement between theory and experiment was obtained. The extension of the IBFM calculations to lighter $N=59$ isotones is consistent with the recent discovery of coexisting structures and dual double-subshell closure in respective even-even core nuclei. [S0556-2813(96)02511-3]

PACS number(s): 21.60.Fw, 23.40.−s, 23.20.Lv, 27.60.+j

I. INTRODUCTION

The interacting boson model for even-even nuclei has been shown to be able to account for the structure of nuclei as they change from vibrational to rotational character and thus provide the capability of describing a wide variety of transitional nuclei. The extension of this model to odd-mass nuclei provides the means to account for structures of an even wider range of nuclei. The odd-mass isotones with $N=59$ serve as a good test of the odd-mass boson-fermion model. In this series of isotones the 59th neutron observes a rapidly changing $N=58$ core which goes from proton shell closure at $Z=50$ to six proton pairs less at ^{96}Sr which has been shown to possess shape coexistence. There are dramatic changes in the pattern of low-energy levels of the $N=59$ isotones. Of particular note is the abrupt change in the structure between ^{103}Ru and ^{105}Pd which are the $Z=44$ and 46 isotones, respectively, and between ^{99}Zr and ^{101}Mo which are $Z=40$ and 42 isotones. We have undertaken investigations of the low-energy level properties of the $N=59$ isotones and have given a preliminary survey of our results elsewhere [1] while details concerning the interacting boson-fermion model can be found, for example, in Refs. [2,3].

In general, heavy-ion reaction studies favor the population of high-spin states which tend to be the aligned members of particle-core multiplets [4,5]. For ^{105}Pd recent studies have focused on the high-spin states. The decay of $1/2^-$ 41.0-day ^{105}Ag^g is one of the few cases where low-spin levels in any of the odd-mass Pd nuclei can be studied.

Data on the $A=105$ mass chain have been previously compiled in Nuclear Data Sheets [6]. Previous decay studies of 41.0-day ^{105}Ag^g have included detailed conversion electron studies [7,8], two studies of angular correlations [9,10], and gamma-ray studies [8,11,12]. However, in spite of all these studies, a large number of discrepancies still exist including spin-parity assignments for several levels. In addition, previous studies have not been sensitive enough to observe low-intensity gamma rays which represent transitions between known levels. By producing 41.0-day ^{105}Ag^g from the decay of ^{105}Cd [which was in turn produced via the ^{106}Cd$(n,2n)$ reaction], we have been able to observe 17 previously unobserved gamma rays, for 14 of which only conversion electron data have been previously available. New data have allowed us to establish new spin-parity assignments for the 921 keV and 962 keV levels and to identify two new levels in ^{105}Pd. The decay of the $7/2^+$, 7.23-min ^{105}Ag^m isomer has been studied by Krien *et al.* [13] and reviewed by Abukhov *et al.* [14]. By observing this decay in transient equilibrium with 55.5-min ^{105}Cd sources, we have determined a new, more accurate value for the positron-to-electron capture branch for ^{105}Ag^m of 1.8(2)%.

II. EXPERIMENTAL PROCEDURE

The sources used in this study were produced by irradiating 50–100 mg samples enriched to 82.09% ^{106}Cd as the oxide with 14-MeV neutrons for the Lawrence Livermore National Laboratory (LLNL) insulated-core-transformer (ICT) accelerator with a rotating target neutron source (RTNS). The RTNS produces 14-Mev neutrons with the ^{2}H(^{3}H,^{4}He)n reaction and can attain a maximum flux of $\sim 6\times 10^{12}$ n/sec into 4π.

Starting approximately 20 min after irradiation, direct gamma-ray spectra were taken to observe the gamma rays resulting from the decay of 7.23-min ^{105}Ag^m in transient equilibrium with its ^{105}Cd parent. A large number of detector-analyzer systems were used, including a Compton suppression spectrometer. These systems and the counting conditions are described elsewhere [15]. The intensities of

 © 1996 The American Physical Society

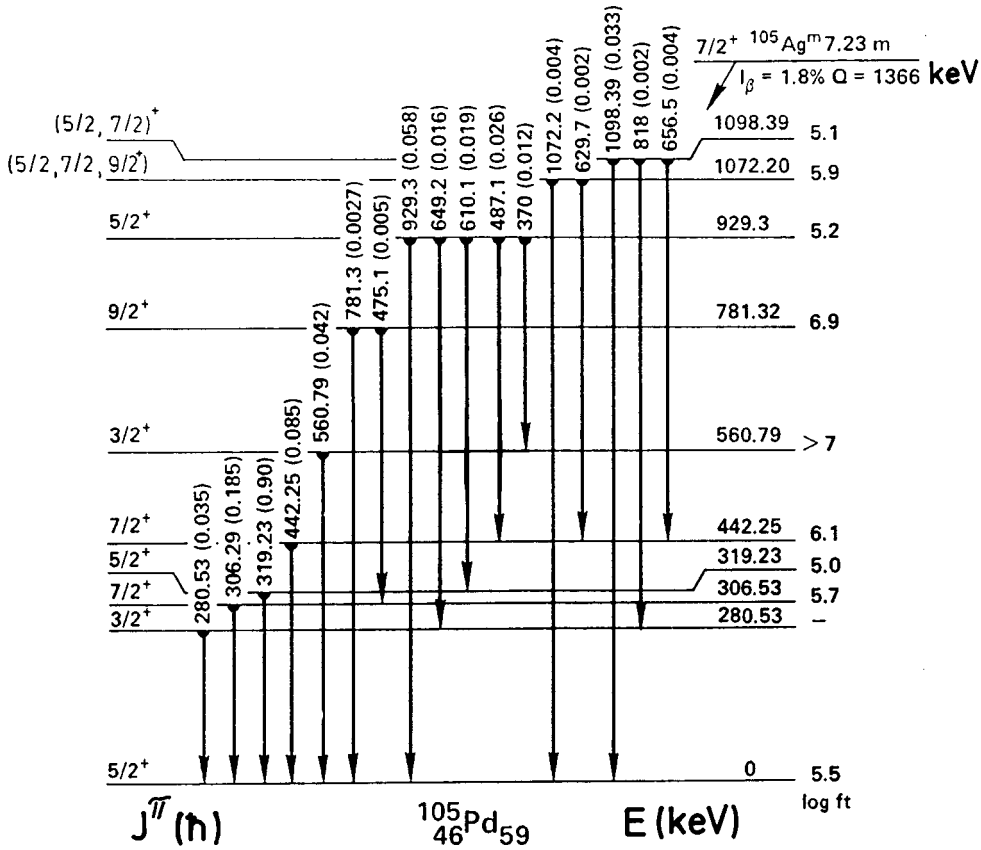

FIG. 1. Decay scheme for $^{105}Ag^m$.

$^{105}Ag^m$ gamma rays relative to ^{105}Cd were determined solely from counts started at least 90 min after the end of irradiation, at which time the condition of transient equilibrium was in effect.

Following the early measurements, two sources were allowed to decay for ~20 days and then observed with two different detector systems: (i) a 50-cm^3 Ge(Li) detector and (ii) a 2.5-cm^3 Ge (Li) x-ray detector. Counting periods of 1200 and 5000 min were taken every 7 days for a period of 5 weeks. For the large detector, source-detector distances were >10 cm to minimize gamma-ray summing effects. The principle activity present in these sources was 41.0-day $^{105}Ag^g$. The following contaminating activities were readily identified and their well-documented gamma rays deleted from the results: 8.41-day $^{106}Ag^m$, 44.6-day $^{115}In^m$, 453-day ^{109}Cd, and 252-day $^{110}Ag^m$.

In both portions of this study, a gamma-ray photopeak analysis was performed using the LLNL spectrum analysis code GAMANAL [16]. The gamma-ray energies were obtained by counting sources simultaneously with numerous multi-gamma-ray source standards.

III. EXPERIMENTAL RESULTS

A. Decays of 7.23-min $^{105}Ag^m$ and of 41.0-day $^{105}Ag^g$

In observing the decay of mixed ^{105}Cd and $^{105}Ag^m$, 274 gamma rays were identified as belonging to the decay of ^{105}Cd. After correcting for the decay of 41.0-day $^{105}Ag^g$ we could identify the gamma rays of $^{105}Ag^m$ (Fig. 1). In our previous work on the decay of ^{105}Cd we were able to determine that $(85.3\pm1.8)\%$ of all ^{105}Cd decays populate the 25-keV isomer of ^{105}Ag. Using the half-life values [6] of 55.5 min and 7.23 min for ^{105}Cd and $^{105}Ag^m$, respectively, and assuming transient equilibrium, we calculate that there are 9.04 ± 0.11 319-keV gamma rays per 1000 decays of $^{105}Ag^m$ (cf. Krien *et al.* [13], who report an absolute intensity for the 319-keV gamma ray of 0.48). Using our value, we calculate the positron-to-capture branch of 7.23-min $^{105}Ag^m$ as $(1.8\pm0.8)\%$.

A total of 59 gamma rays were attributed to the decay of 41.0-day $^{105}Ag^g$ (Fig. 2). Three additional transitions for which we do not observe gamma rays have been observed in earlier conversion electron measurements [7,8]. However, we are able to set limits on their occurrence in the spectra. The multipolarities of transitions are displayed in Table I. These were determined using our gamma-ray intensities, previous conversion electron intensities [7,8], and theoretical conversion electron coefficients [17]. The 187-keV transition was observed only in the conversion electron measurements of Suter *et al.* [7] and our gamma-ray intensity requires that any such transition would have to possess a multipolarity of $M2$, $E3$, or higher multipolarity. The 709-keV transition was observed as a gamma ray, but with large uncertainty in our measurements and its present assignment as a $^{105}Ag^g$ gamma ray is doubtful.

We have eliminated 11 previously reported transitions: 178.34, 186.64, 285.9, 286.7, 350.5, 402.8, 580, 582, 636.6, 796, and 860 keV.

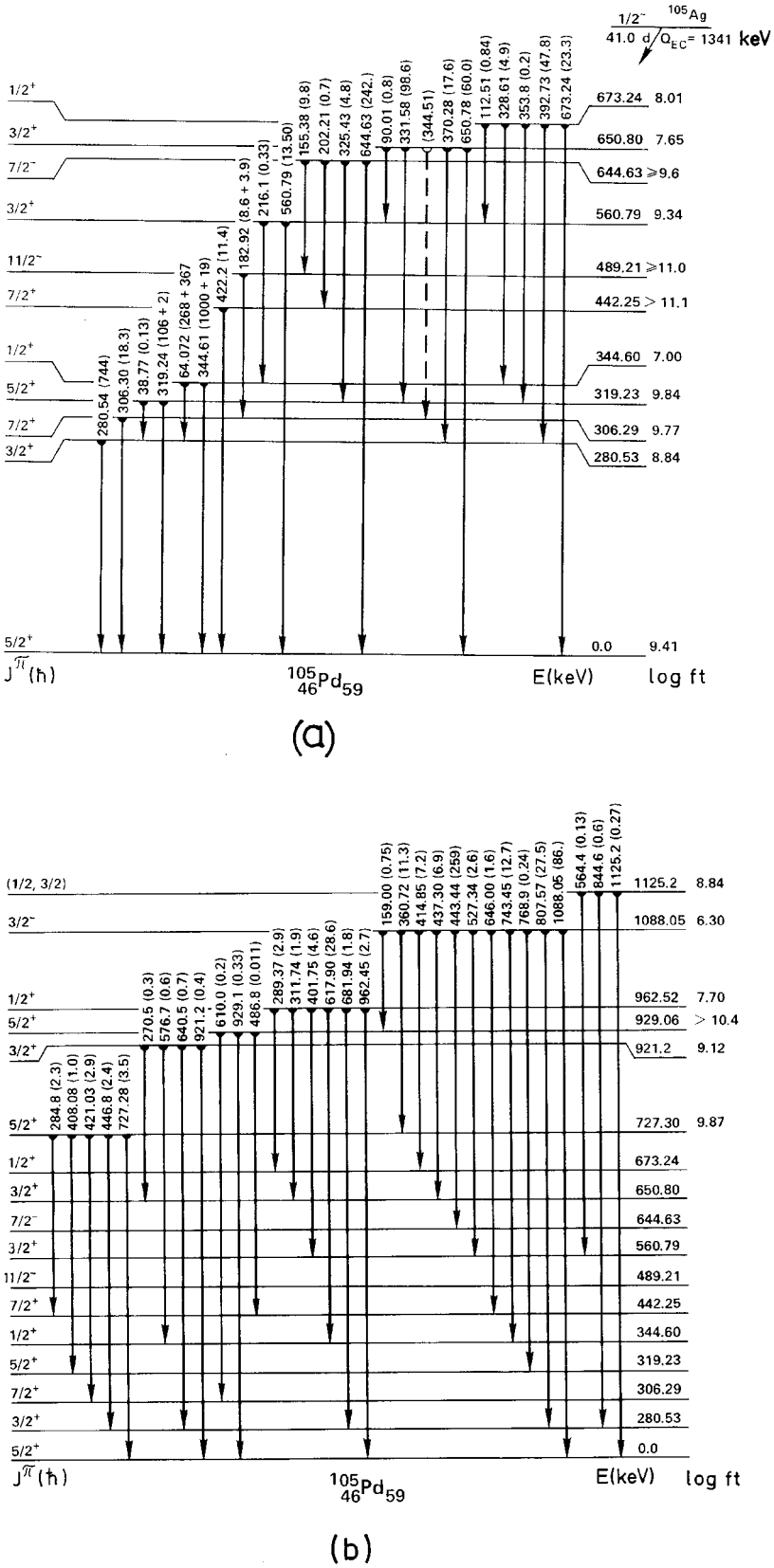

FIG. 2. Decay scheme for $^{105}Ag^{g}$: (a) levels up to 700 keV, (b) levels above 700 keV.

B. Levels of ^{105}Pd observed in decays of $^{105}Ag^{m,g}$

In Fig. 1 we present the composite decay scheme of $^{105}Ag^{m}$ which is in accordance with the basic decay scheme reported by Krien *et al.* [13] and by Abukhov *et al.* [14]. However, we do place a previously unobserved 370-keV transition as populating the known $3/2^{+}$ level at 560 keV. The logft values were calculated using the half-life value of 7.23 min, the Q_{EC} value of 1366 keV [15,18], our new value of $(1.8\pm0.2)\%$ for the total (positron+electron caputre) branch, and the logft tables of Gove and Martin [19].

TABLE I. Multipolarities assigned to transitions. Decay of 41.0-day $^{105}Ag^{g}$.

Assignment From	To	Multipole [a]
319	280	$M1$
344	280	$M1$
650	560	$M1$
673	560	$M1$
644	489	$E2$
489	306	$M2$
644	442	$E1$ or $M1$
560	344	$E2$
921	650	
280	g.s.	$M1+(0-12\,\%)E2$
727	442	$M1$
962	673	
306	g.s.	$M1$
962	650	$M1$
319	g.s.	$M1$
644	319	$E1$
673	344	$M1$
650	319	$M1$
344	g.s.	$E2$
650	306	
673	319	
1088	727	$E1$
921	280	
644	g.s.	$E1$
1088	442	$M2$
650	g.s.	$M1(E2)$
673	g.s.	$M1(E2)$
962	280	$M1(E2)$
727	g.s.	$M1$
1088	344	$E1$
1088	306	
1088	280	$E1$
1125	280	
921	g.s.	
929	g.s.	$E2$
962	g.s.	
1088	g.s.	$E1$
1125	g.s.	

[a]Based on our gamma-ray data and the conversion electron intensities of Kawakami and Hisatake [8].

In Fig. 2 we present the decay scheme of 41.0-day $^{105}Ag^{g}$ to levels of ^{105}Pd. The levels observed in this decay, along with their properties, are tabulated in Table II. The absolute decay branch to the ground state of ^{105}Pd was determined from the positron measurements of Pierson and Rengan [20] (positron to 280-keV gamma-ray intensity ratio of 2.7×10^{-5}) and the tables of Gove and Martin [19]. The absolute electron capture (EC) branch to each of the excited states was determined via a detailed balance of the intensities of the transition populating and depopulating the level, with the conversion electron contribution of each transition calculated using the theoretical total conversion coefficient [17] for the multipolarity assigned in Table I. The $\log ft$ values were calculated using the adopted half-life value of 41.0 days [6], the Q_{EC} value of 1341 ± 9 of Wapstra and Audi [18], and the tables of Gove and Martin [19].

We have observed some previously unreported transitions in the decay of $^{105}Ag^{g}$ and have placed these in the decay scheme on the basis of energy sums. Two were placed between previously known levels, six established two new levels, and the final two depopulating a level previously proposed in the decay of $^{105}Ag^{m}$ and via (p,d) and (d,t) transfer reaction studies [21–23]. For each of these ten transitions a reasonable estimate of the upper limit for the K conversion electron intensity was obtained by examining the data of Kawakami and Hisatake [8] and resulted in setting the transition multipolarity as either $E1$ or $M1/E2$. The placement of each of these transitions was found to be consistent with the deduced multipolarity.

The composite level scheme for ^{105}Pd as observed in the decays of the $^{105}Ag^{m}$ and $^{105}Ag^{g}$ contains two new spin-parity assignments in comparison to the level scheme presented in the last Nuclear Data Sheets (NDS) compilation [24].

The 921-keV level. We place this level on the basis of four newly observed transitions in decay of $^{105}Ag^{g}$. The $\log ft$ value of 9.12, the $l=2$ angular distribution (and lack of $l=0$ component) at 925 keV in reaction studies, and the gamma-ray branching lead to a $3/2^{+}$ assignment.

The 962-keV level. This level has a spin-parity value of $1/2^{+}$ based on the observed $l=0$ angular distribution in (d,p) transfer reaction studies [25]. We note that our measurement of pure $E2$ multipolarity for the 962-keV level resolves the problem of two levels at around 962 keV expected in Nuclear Data Sheets [26]. We thus establish only a single $1/2^{+}$ level at this energy.

IV. CALCULATION FOR POSITIVE-PARITY LEVELS OF ^{105}Pd IN THE INTERACTING BOSON-FERMION MODEL

The even-even core nucleus ^{104}Pd has been described in the interacting boson model (IBM) [27–29] and the odd-even nucleus ^{105}Pd in the interacting boson-fermion model (IBFM) [30–34]. The core nucleus ^{104}Pd has a closely spaced triplet $0_2^+,2_2^+,4_1^+$. This triplet can be fitted in the U(5) limit of the IBM as a $n_d=2$ multiplet; however, the predicted $n_d=3$ multiplet is in this case nearly degenerate, while the experimental splitting of these states is more than 500 keV. Furthermore, if a $d_{5/2}$ quasineutron is coupled to such a core, a low-energy $9/2^{+}$ level is predicted (at 320 keV), in contradiction to our experimental knowledge and the overall agreement between calculation and experiment is rather poor. Such a parametrization has been studied elsewhere [35]. It turns out that the agreement with the experiment cannot be improved as long as we use the U(5) boson core without n_d mixing in the wave function which has to be used if we want to reproduce a closely spaced triplet $0_2^+,2_2^+,4_1^+$.

In this paper we investigate a different type of the boson core: The core parameters are adjusted to reproduce the group of levels 0_3, 2_3, 3_1, 4_2, and 6_1. [This group of levels resembles the $n_d=3$ quintuplet of the U(5) limit.] The IBM parameters used in our calculation are $h_1=0.54$ MeV,

TABLE II. Population of ^{105}Pd levels in the beta decay of 41.0-day $1/2^-$ ^{105}Ag^g.

Level	J	% Population	logft	logf_1t
0	$5/2^+$	2.9(3)		9.41
281	$3/2^+$	1.1(4)	8.84	
306	$7/2^+$	<0.001	>12	
319	$5/2^+$	0.10(6)		10.43
345	$1/2^+$	66(1)	7.00	
443	$7/2^+$	<0.001	>12	
489	$11/2^-$	<0.004	>11	
561	$3/2^+$	1.8(1)	9.34	
645	$7/2^-$	<0.09	>10	
651	$3/2^+$	7.03(7)	7.65	
673	$1/2^+$	2.80(4)	8.01	
727	$5/2^+$	0.03(1)		10.0
921	$3/2^+$	0.08(1)	9.12	
929	$5/2^+$	$\leqslant 0.0004$		$\geqslant 11.3$
963	$1/2^+$	1.76(3)	7.70	
1088	$3/2^-$	17.6(2)	6.30	
1125	1/2, 3/2	0.04(1)	8.84	

$h_2=-0.08$ MeV, $h_3=0.09$ MeV, $h_{40}=-0.1$ MeV, $h_{42}=-0.1$ MeV, $h_{44}=0.32$ MeV, and $N=6$. Here, the h_i parameters are defined as in Ref. [33]. The relation to the standard IBM parameters from Ref. [29] is

$$h_1=\epsilon_d-\epsilon_s+\left(\frac{1}{\sqrt{5}}u_2-u_0\right)(N-1), \tag{1}$$

$$h_2=\frac{1}{\sqrt{2}}\tilde{v}_0, \tag{2}$$

$$h_3=\tilde{v}_2, \tag{3}$$

$$h_{4L}=\sqrt{2L+1}\left(\frac{1}{2}c_L-\frac{1}{\sqrt{5}}u_2+\frac{1}{2}u_0\right). \tag{4}$$

The low-energy part of the IBM level spectrum of the core is presented in Fig. 3 and compared to the levels of ^{104}Pd which have been experimentally identified [26].

It should be noted that for this parametrization the calculated $0_2,2_2,4_1$ triplet has a splitting of 0.25 MeV, which is much more than experimentally observed. On the other hand, the IBM wave functions associated with this parametrization exhibit sizable mixing of components with different number of d bosons (n_d). This is seen from the wave functions presented in Table III. The IBM wave functions are expressed in s,d-boson basis

$$|I\rangle=\Sigma_{n_d v}\xi^I_{n_d v}|n_d v I\rangle. \tag{5}$$

Here, $|n_d v I\rangle$ denotes the IBM basis state with $N-n_d$ s boson and n_d d bosons coupled to the angular momentum I. The seniority quantum number v is an additional quantum number which serves to distinguish between different states having the same values of n_d and I.

We note that the n_d mixing in the IBM wave functions plays a much more important role in the structure of ensuing IBFM wave functions than the precise energies of the 0_2, 2_2, and 4_1 levels. Therefore, as will be seen, a rather good agreement between theory and experiment can be obtained for the states in ^{105}Pd below 0.5 MeV.

The present IBM parametrization corresponds to a somewhat distorted U(5) boson system. Accordingly, the states of the ground-state band $0_1,2_1,4_1,\ldots$ are dominated by components $|n_d I\rangle=|00\rangle, |12\rangle, |24\rangle, \ldots$, respectively. However, because of violation of U(5) symmetry, there are sizable admixtures, in particular the $\Delta n_d=2$ admixtures.

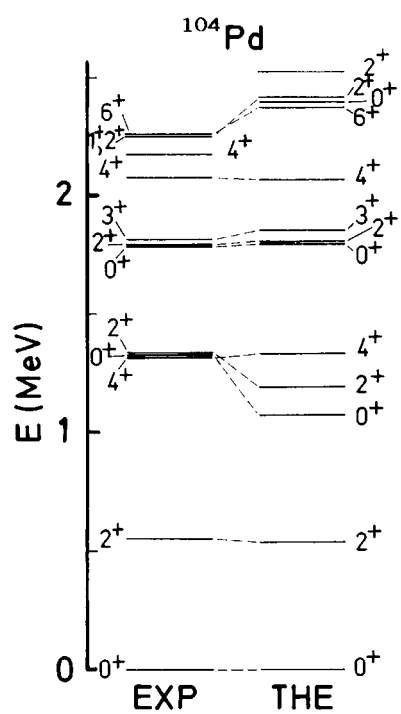

FIG. 3. Comparison of experimentally known levels of ^{104}Pd with the levels fitted by the IBM core.

TABLE III. Wave functions of the 0_1^+, 2_1^+, 2_2^+, and 4_1^+ states of the ^{104}Pd boson core. Only components with amplitudes larger than 1% are listed.

n_dI [a]	0_1^+ ξ_{n_dI}	n_dI	2_1^+ ξ_{n_dI}	2_2^+ ξ_{n_dI}	n_dI	4_1^+ ξ_{n_dI}
00	0.83	12	0.82	0.35	24	0.83
20	−0.52	22	−0.28	0.85	34	−0.36
30	−0.11	32	−0.46		44	−0.40
40	0.16	42	0.14	−0.39	54	0.13
		52	0.11			

[a]The following notation is employed: n_dI denotes the IBM boson state $|n_d\, v_{\text{lowest}} I\rangle$, where n_d stands for the number of d bosons and v_{lowest} for the lowest seniority associated with given values of n_d and I. Otherwise, we abreviate $|n_d v' I\rangle$ by $|n_d I'\rangle$, where $v' > v_{\text{lowest}}$.

As a further test of present IBM parametrization for the ^{104}Pd core nucleus, we have calculated the corresponding γ-decay pattern for the low-lying levels. The results are presented in Table IV, in comparison to the experimental data for ^{104}Pd.

In the IBFM calculation for the positive-parity states in ^{105}Pd we include the neutron quasiparticle states $\tilde{d}_{5/2}$, $\tilde{g}_{7/2}$, $\tilde{s}_{1/2}$, and $\tilde{d}_{3/2}$ where the energies (relative to the $\tilde{d}_{5/2}$ state) are 0, 0.25, 0.35, and 0.6 MeV, respectively, and the corresponding occupation probabilities are 0.85, 0.4, 0.1, and 0.05, respectively. The boson-fermion interaction strengths are $A_0 = -0.01$ MeV, $\Gamma_0 = 0.11$ MeV, $\Lambda_0 = 1.4$ MeV, and $\chi = -\sqrt{7}/2$. These parameters are defined according to Ref. [33], coinciding with standard IBFM definitions for Γ_0, Λ_0, and χ from Ref. [30] and for A_0 from Ref. [34]. The radial integrals of r^2 were calculated using harmonic oscillator wave functions.

The calculated positive-parity spectrum is presented in Fig. 4 and compared to the experimental data. In Table V the main components in the wave functions of low-energy positive-parity states are presented. The wave functions are expressed in the standard IBFM basis:

TABLE IV. Calculated γ-decay pattern for low-lying levels in ^{104}Pd in comparison to data.

I of level From	To	I_γ Theor. [a]	Theor. [b]	Expt. [c]
2_2^+	0_1^+	26	213	86
	2_1^+	100	100	100
	4_1^+	0.0	0.0	-
	0_2^+	0.0	0.0	-
0_3^+	2_1^+	100	100	100
	2_2^+	67	1	9.4
2_3^+	0_1^+	213	32	10
	2_1^+	100	100	100
	4_1^+	583	4	-
	0_2^+	1258	8	3
	2_2^+	387	3	-
	0_3^+	0.0	0.0	-

[a]$\chi' = 0$ (see Sec. IV).
[b]$\chi' = -0.2$.
[c]Ref. [26].

$$|J_r\rangle = \Sigma_{jn_dvI}\xi^{J_r}_{jn_dvI}|\tilde{j}, n_dvI; J\rangle. \tag{6}$$

Here $|J_r\rangle$ denotes the rth state of angular momentum J, j labels the quasiparticle state, and n_dvI the IBM boson state. The angular momenta j and I are coupled to the total boson-fermion angular momentum J.

Comparing IBFM wave functions of the low-lying states in ^{105}Pd (Table V) and the IBM wave functions of the members of ground-state band in ^{104}Pd (Table III), it is seen that the main structure of the calculated IBFM wave functions of the levels in ^{105}Pd can be approximately presented in the form of quasiweak-coupling basis states as follows:

$$|5/2_1^+\rangle \approx \{\tilde{d}_{5/2}|0_1\rangle\}_{5/2}, \tag{7}$$

$$|3/2_1^+\rangle \approx \{\tilde{d}_{5/2}|2_1\rangle\}_{3/2}, \tag{8}$$

$$|7/2_1^+\rangle \approx \{\tilde{g}_{7/2}|0_1\rangle\}_{7/2}, \tag{9}$$

$$|5/2_2^+\rangle \approx \{\tilde{g}_{7/2}|2_1\rangle\}_{5/2}, \tag{10}$$

$$|1/2_1^+\rangle \approx \{\tilde{s}_{1/2}|0_1\rangle\}_{1/2}, \tag{11}$$

$$|7/2_2^+\rangle \approx \{\tilde{d}_{5/2}|2_1\rangle\}_{7/2}. \tag{12}$$

Here $|0_1\rangle$ and $|2_1\rangle$ denote the IBM wave functions of the boson core, which are given in Table III.

For example, if we use the IBM wave function of the 0_1 state from Table III, we obtain the quasiweak-coupling state $\{\tilde{d}_{5/2}|0_1\rangle\}_{5/2}$ expressed in the fermion-boson basis of the IBFM:

$$\{\tilde{d}_{5/2}|0_1\rangle\}_{5/2} = 0.83|\tilde{d}_{5/2}, 00; 5/2\rangle - 0.52|\tilde{d}_{5/2}, 20; 5/2\rangle - 0.11|\tilde{d}_{5/2}, 30; 5/2\rangle + 0.16|\tilde{d}_{5/2}, 40; 5/2\rangle.$$

On the other hand, the corresponding components in the IBFM wave function of $5/2_1$ state from Table V read

$$|5/2_1\rangle = 0.80|\tilde{d}_{5/2}, 00; 5/2\rangle - 0.45|\tilde{d}_{5/2}, 20; 5/2\rangle - 0.10|\tilde{d}_{5/2}, 30; 5/2\rangle + 0.13|\tilde{d}_{5/2}, 40; 5/2\rangle.$$

These components amount to 87% of the total IBFM wave function. Among the remaining components in the IBFM wave function, the largest are $0.23|\tilde{d}_{5/2}$,

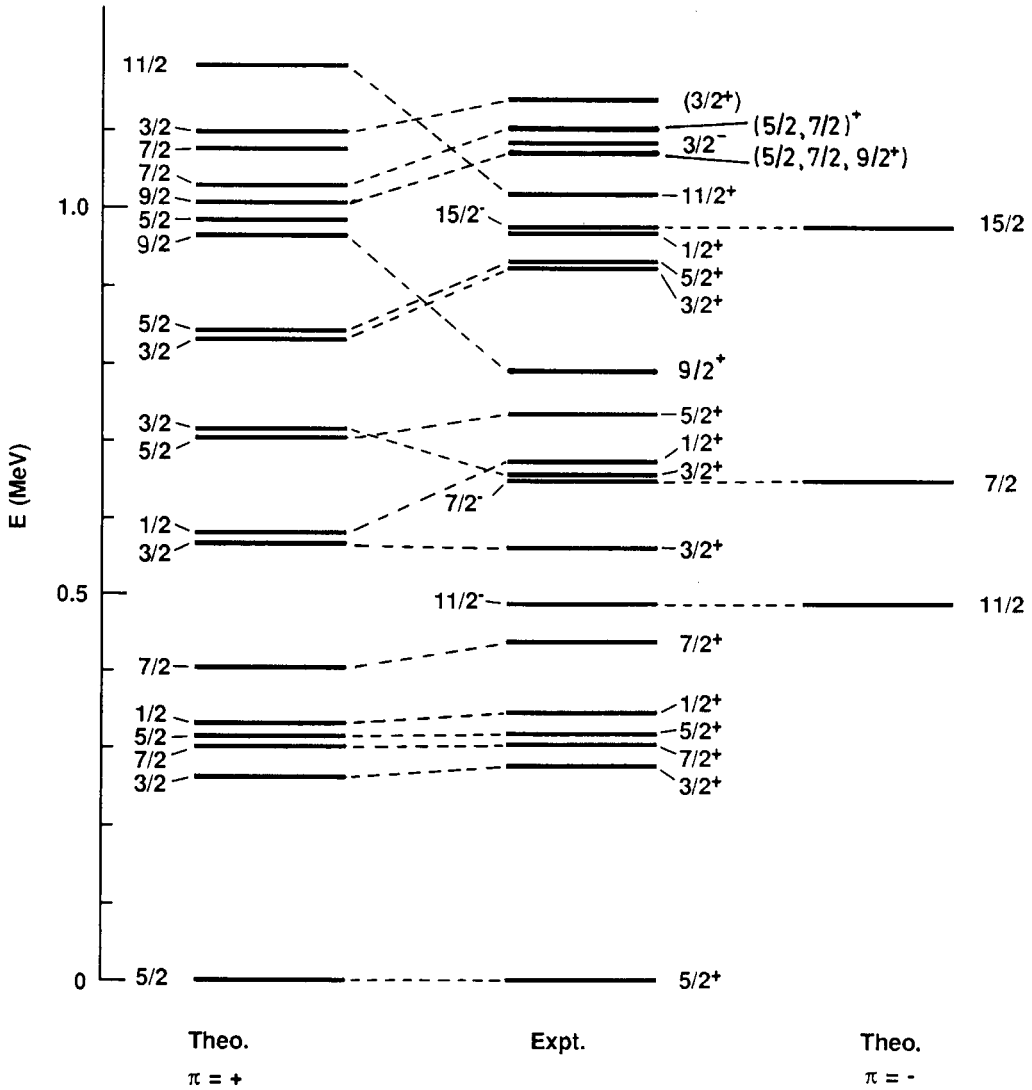

FIG. 4. Comparison of levels of ^{105}Pd predicted by the IBFM calculation with the experimentally known levels up to 1200 keV.

$12;5/2\rangle - 0.17\,|\tilde{d}_{5/2},\,22;5/2\rangle$ and $-0.12|\tilde{d}_{5/2},\,32;5/2\rangle$. In the quasiweak-coupling scheme these components are associated with the admixture of $\{\tilde{d}_{5/2}|2_1\rangle\}_{3/2}$ quasiweak-coupling components.

A similar situation appears for the $3/2_1^+$ state. In this case 85% of the total strength in the IBFM wave function corresponds to components which can be associated with $\{d_{5/2}|2_1\rangle\}_{3/2}$ quasiweak-coupling state. Among the admixed components the three largest (amouting to 7% in total) contain the $\tilde{g}_{7/2}$ quasiparticle.

Inspecting the IBFM wave functions of the states $7/2_1^+$, $5/2_2^+$, $1/2_1^+$, and $7/2_2^+$ in Table V, it is seen that 91%, 66%, 60%, and 90% of the total strength in the wave functions can be associated with the weak-coupling classification (9), (10), (11), and (12), respectively.

A rather sensitive test of particular components in the wave functions are the spectroscopic factors. Using the calculated wave functions and the transfer parameter [36,37] $\gamma_0 = 0.2$, we compute the spectroscopic factors $(2J+1)S_{d,p}$. In Table VI we present the calculated spectroscopic factors for a few low-lying positive-parity levels. It should be noted that the only free parameter in the calculation of the spectroscopic factors is $\gamma_0 = 0.2$. Its value is close to the value $\gamma_0 = 0.23$ used in the previous calculation for ^{57}Co [36].

The unique first-forbidden (UFF) beta population of the lowest $5/2^+$ levels also support the model calculations. The beta population by UFF transitions is governed by a single matrix element. Hence, unlike allowed first-forbidden beta decay which is governed by several matrix elements, UFF reduced transition values ($\log f_1 t$) are indicative of structural changes. Since the parent ground state is $s_{1/2}$, we should expect the allowed UFF transitions to occur to $d_{5/2}$ associated levels (UFF allows a J value change of 2 units) but should expect highly hindered transitions to $g_{7/2}$ related levels. As shown in Fig. 5, the $\log f_1 t$ value of 9.41 to the $5/2^+$ gs is consistent with predominatly $d_{5/2}$ core-coupled character of this level and the factor of 10 increase in the UFF hindrance to the 319-keV level with a $\log f_1 t$ value of 10.43 is consistent with the prediction that this level has mostly a $g_{7/2}$ core-coupled nature. (It should be noted that the IBFM-PTQM boson-fermion interaction causes the $g_{7/2}$-

TABLE V. Wave functions of low-lying positive-parity states of ^{105}Pd. Only components with amplitudes larger than 1% are listed.

J_r	$j\ n_d\ I$ [a]	$\xi^{J_r}_{jn_dI}$
$5/2_1^+$	$d_{5/2}$,00	0.80
	$d_{5/2}$,12	0.23
	$d_{5/2}$,20	−0.45
	$d_{5/2}$,22	−0.17
	$d_{5/2}$,32	−0.12
	$d_{5/2}$,40	0.13
$3/2_1^+$	$d_{5/2}$,12	0.78
	$d_{5/2}$,22	−0.26
	$d_{5/2}$,32	−0.40
	$d_{5/2}$,42	0.12
	$g_{7/2}$,12	−0.20
	$g_{7/2}$,24	−0.11
	$g_{7/2}$,32	0.12
	$s_{1/2}$,12	0.12
$7/2_1^+$	$d_{5/2}$,12	0.17
	$g_{7/2}$,00	0.84
	$g_{7/2}$,20	−0.44
	$g_{7/2}$,24	−0.12
	$g_{7/2}$,40	0.12
$5/2_2^+$	$d_{5/2}$,00	−0.21
	$d_{5/2}$,12	0.36
	$d_{5/2}$,22	−0.12
	$d_{5/2}$,24	0.11
	$d_{5/2}$,32	−0.21
	$g_{7/2}$,12	0.70
	$g_{7/2}$,22	−0.19
	$g_{7/2}$,32	−0.37
	$s_{1/2}$,12	0.14
$1/2_1^+$	$d_{5/2}$,12	0.37
	$d_{5/2}$,22	−0.18
	$d_{5/2}$,32	−0.17
	$s_{1/2}$,00	−0.69
	$s_{1/2}$,20	0.35
	$d_{3/2}$,12	−0.38
	$d_{3/2}$,32	0.19
$7/2_2^+$	$d_{5/2}$,12	0.83
	$d_{5/2}$,22	−0.17
	$d_{5/2}$,24	0.10
	$d_{5/2}$,32	−0.43
	$g_{7/2}$,00	−0.16

[a]Extending the notation from Table III, we denote the basis states $|\tilde{j},n_d\ v_{\rm lowest}I;J\rangle$ by $\tilde{j}n_dI$ and the basis states $|\tilde{j},n_dv'I;J\rangle$ (where v' denotes the seniority which is larger than $v_{\rm lowest}$ for given values of n_d and I) by $\tilde{j}n_dI'$.

$d_{5/2}$ mixing; however, because of the spin-flip matrix elements, the calculated mixing turns out to be rather small.) If we use the ratio of $|\tilde{d}_{5/2},00\rangle$ components, we predict a UFF ratio of 0.636/0.045 =14, in close agreement with the observed ratio of 10.5. Although the allowed first-forbidden beta transitions cannot be used as a good indication of structural effects, the trend in the first-forbidden beta strength does reflect the major character of the levels: i.e., the fastest is to the level with predominately $s_{1/2}$ character, the transitions to the predominately $d_{5/2}$ character levels are an order of magnitude slower, and those to the predominately $g_{7/2}$ character levels are another order of magnitude slower.

TABLE VI. Calculated spectroscopic factors of four low-lying positive-parity states in comparison with experimental data [24].

J	$(2J+1)\ S_{d,p}$ Theor.	Expt.
$3/2_1^+$	0.07	
$5/2_1^+$	0.97	1.24
$5/2_2^+$	0.10	
$7/2_1^+$	4.21	5.22

In Table VII we present the electric quadrupole and magnetic dipole moments, calculated by using IBFM wave functions of ^{105}Pd and the standard IBFM forms for $E2$ and $M1$ operators. In this calculation the boson effective charge $e^{\rm vib}=1.25$ and $\chi=-0.9$ are taken from the previous IBM calculation [38] for ^{102}Ru. Here, the effective charges end gyromagnetic ratios are defined according to Ref. [33]. In the calculation of $E2$ properties we have included an additional term in the $E2$ operator which in IBM representation has the form

$$e^{\rm vib}\frac{3}{4\pi}R_0^2\chi'[(d^+d^+)_2ss+s^+s^+(dd)_2],$$

with $\chi'=-0.4$ [33,39]. For neutrons we use the standard value for the effective charge $e^{sp}=0.5$. The gyromagnetic ratios $g_R=0.6$, $g_l=-0.1$, and $g_s=0.3g_s^{\rm free}$ have been taken from the previous calculation [40] for the neighboring odd-even nucleus ^{103}Ru.

In Table VIII we present the calculated branching ratios corresponding to the same parametrization as used for the static moments. The calculated results are compared with the present experimental data. The experimental decay pattern is reasonably well reproduced. The calculated half-lives of the low-energy states are presented in Table IX and compared to the experimental data. The largest $E2$ reduced transition probability among the low-energy states is associated with the $7/2_2^+\rightarrow 5/2_1^+$ transition. This is a consequence of the structure of wave functions of the $5/2_1$ and $7/2_2$ states which are dominated by $|\tilde{d}_{5/2},00;5/2\rangle$ and $|\tilde{d}_{5/2},12;7/2\rangle$ components, respectively.

V. NEGATIVE-PARITY STATES AND THE OCCURRENCE OF A 3/2$^-$ INTRUDER STATE

The character of the collective negative-parity spectrum of ^{105}Pd is obfuscated by the intrusion of an unexpected $3/2^-$ level at 1088 keV. This level, if included as a $h_{11/2}$ core-coupled state, has led to misleading results in earlier calculations using a symmetric rotor picture [5]. We show the gamma-deexcitation and beta-population properties of this level in Fig. 5. Of particular importance is our identification of a 646-keV gamma ray. When we use our gamma-ray intensities in combination with the conversion electron measurements of Kawakami and Hisatake [8], we find a $M2$ multipolarity for this transition. There is no level life-

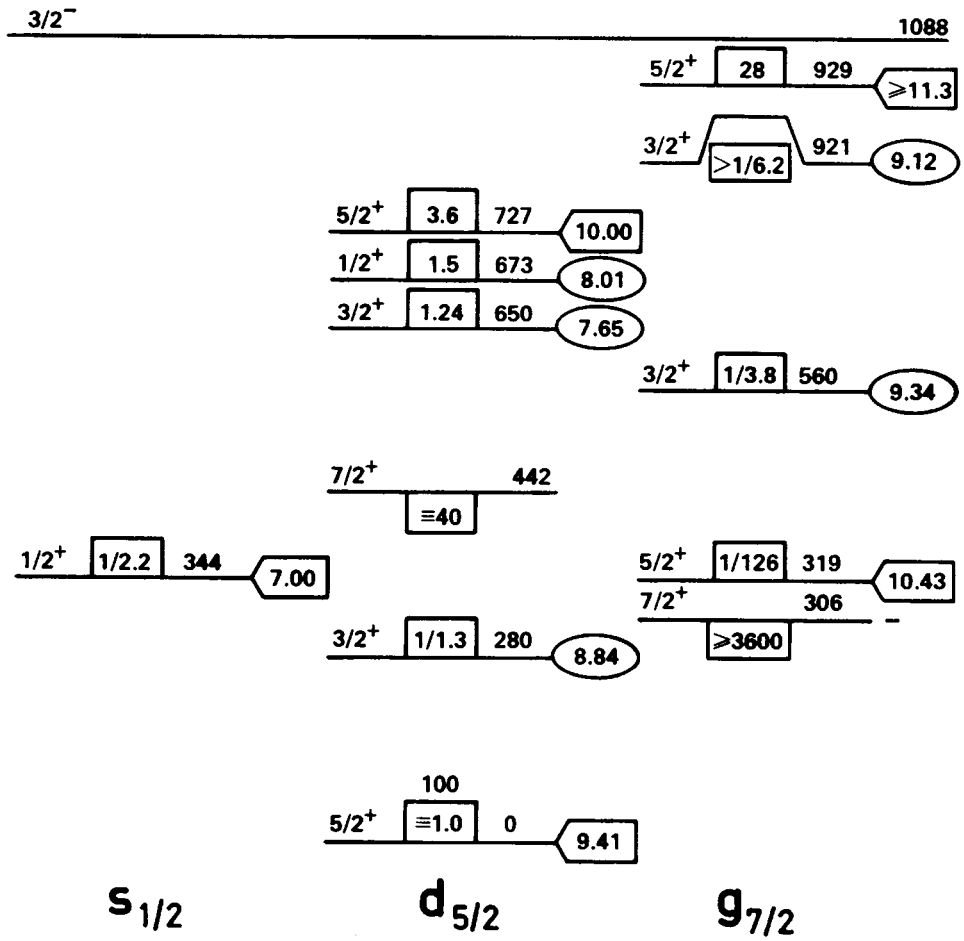

FIG. 5. Deexcitation properties of the 1088-keV $3/2^-$ level in ^{105}Pd.

time measurement for this level. However, if we use the relative hindrances known for the $M2$ transition in this region as given by Andrejtscheff *et al.* [41], we can estimate the level lifetime and transition rates of deexciting transitions. Such an estimate leads to the result that instead of being collective, the 446-keV $E2$ transition to the $7/2^-$ level is at least 20 times slower than the $E2$ transition between the 644-keV $7/2^-$ level and its associated $11/2^-$ bandhead at 489 keV. Also, the limit that we place on the intensity of a transition to the lowest-energy $7/2^+$ level gives a hindrance factor that is at least 90 times slower than the $M2$ transition to the second excited $7/2^+$ level. This and the relative $E1$ transition strengths to the lower-energy level leads us to suggest that the 1088-keV level has a $p_{3/2}$-hole character. Such a configuration would allow less retarded transitions to the $d_{5/2}$-related levels rather than to the $g_{7/2}$-related levels. Thus

TABLE VII. Calculated electric quadrupole and magnetic dipole moments of ^{105}Pd in comparison with experimental data [24].

	$Q(e\text{b})$		μ (μ_N)	
Level	Theor.	Expt.	Theor.	Expt.
$5/2_1^+$	+0.59	+0.66(11)	−0.65	−0.64
$3/2_1^+$	+0.42		−0.23	−0.074(13)
$7/2_1^+$	−0.13		+0.12	
$5/2_2^+$	−0.30		+0.34	+0.95(20)
$1/2_1^+$	−		−0.33	
$7/2_2^+$	+0.03		+0.26	
$11/2_1^-$	−0.59		−1.04	
$7/2_1^-$	−0.56		−1.91	−1.49(9)
$15/2_1^-$	−1.03		+0.14	
$9/2_1^-$	+0.15		−1.21	

TABLE VIII. Calculated $E2$ and $M1$ branching ratios in ^{105}Pd in comparison with experimental data. (See Fig. 4 for association between theoretical and experimental states.)

J of Level		I_γ	
From	To	Expt.	Theor.
$3/2_1^+$	$5/2_1^+$	100	100
$7/2_1^+$	$3/2_1^+$		0.0005
	$5/2_1^+$	100	100
$5/2_2^+$	$7/2_1^+$		0.0002
	$3/2_1^+$	0.12	0.7
	$5/2_1^+$	100	100
$1/2_1^+$	$5/2_2^+$		0
	$3/2_1^+$	27	93
	$5/2_1^+$	100	100
$7/2_2^+$	$5/2_2^+$		2
	$7/2_1^+$		0.0006
	$3/2_1^+$		0.03
	$5/2_1^+$	100	100
$3/2_2^+$	$7/2_2^+$		0.0005
	$1/2_1^+$	2.4	1
	$5/2_2^+$		2
	$7/2_1^+$		0.005
	$3/2_1^+$		0.4
	$5/2_1^+$	100	100
$3/2_3^+$	$3/2_2^+$	0.8	0.4
	$7/2_2^+$		0.08

the observed $M2$ transition (which will have a hindrance of 40 at least [41]) populates the 442-keV $7/2^+$ level which has a predominately $d_{5/2}$ character. We can only place a limit of a hindrance factor (HF) of $\geqslant 3.600$ on any $M2$ transition to the 306-keV $7/2^+$ level which has predominately $g_{7/2}$ character. Also, as shown in Fig. 5, the $E1$ transtions for the deexcitation of the 1088-keV level also reflect the same behavior in that the less favored $E1$ transitions populate the $g_{7/2}$-associated levels while the more favored (less hindered) $E1$ transitions populate those levels with predominately $d_{5/2}$ and $s_{1/2}$ character. Thus the deexcitation properties of the 1088-keV level suggest some $p_{3/2}$ character to the level. Also, as shown in Fig. 6, other low-energy $3/2^-$ levels are known in the neighboring $N=61$ isotones, and as shown by comparison with Fig. 6, their excitation energy correlates with the deformability of the core. However, no experimental transfer data for this state are available [24].

TABLE IX. Calculated half-lives of low-lying levels in ^{105}Pd in comparison with experimental data.

J	Expt. [a]	Theor.
$3/2_1^+$	0.067 ns	0.03 ns
$5/2_2^+$	0.04 ns	0.1 ns
$7/2_2^+$	3.8 ps	7.7 ps
$1/2_1^+$	0.88 ns	0.22 ns
$3/2_2^+$	1.9 ps	6.3 ps
$1/2_2^+$	>2 ps	1.6 ps

[a]Ref. [24].

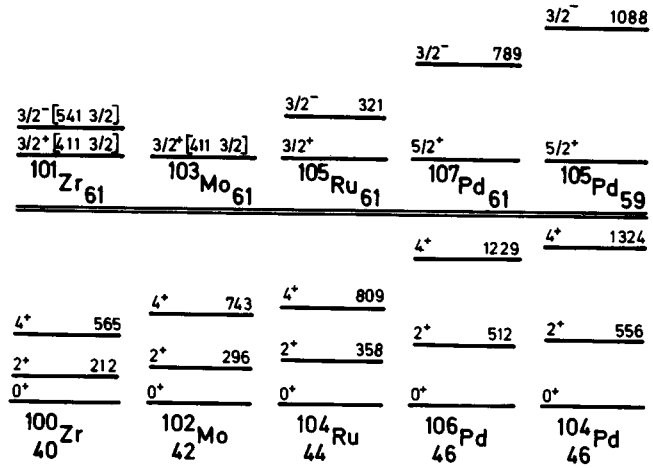

FIG. 6. Experimentally known $3/2^-$ levels in $N=61$ isotones compared with the 1088-keV $3/2^-$ level in ^{105}Pd.

In Fig. 4 we have shown a comparison of the negative-parity level spectrum calculated in IBFM with those known experimentally. Once we exclude the 1088-keV $3/2^-$ level from comparison with IBFM model, the agreement between the calculated negative-parity states (which contain $\tilde{h}_{11/2}$ quasiparticle) and experimental data is rather good. In performing the IBFM calculation we have used an $\tilde{h}_{11/2}$ quasiparticle with the occupation probability of 0.03. In order to reproduce the known $7/2_1^-$ state we have used the interaction strength Γ_0 of 1.2 MeV, while keeping all the other parameters the same as in the calculation for the positive-parity states in ^{105}Pd.

Another consequence of our identification of the 1088-keV level as an intruder state, and not as a member of the $h_{11/2}$ core-coupled family of levels, is that it removes the need to employ a symmetric rotor core as used by Popli and co-workers [5].

VI. STRUCTURAL CHANGES IN THE SEQUENCE OF $N=59$ ISOTONES AND CONCLUSIONS

As shown in Fig. 7, the systematics of the odd-mass $N=59$ isotones exhibits a sudden change in the low-energy positive-parity structure between ^{103}Ru and ^{105}Pd. Elsewhere [40], we have accounted in the IBFM for the positivite-parity states of ^{103}Ru, which arise from recent evaluation of existing and current neutron-capture gamma-ray and beta-decay experiments [40].

The rapid change of structure between ^{105}Pd and ^{103}Ru is reflected, in particular, in the ground-state pattern. In ^{105}Pd the $5/2_1^+$ ground state is rather widely separated from the higher-lying group of levels, while in ^{103}Ru there appears a close-lying doublet $3/2_1^+$, $5/2_1^+$, with $3/2_1^+$ being the ground state. Such a lowering of the $I=j-1$ state associated with the lowest-lying single-particle or quasiparticle configuration of angular momentum j was referred to as the $I=j-1$ anomaly. It has been previously found that this effect appears for seniority three states with the onset of collectivity [42,43]. Similarly, this effect arises in the IBFM due to the exchange force [31]. However, the boson core for ^{103}Ru (i.e.,

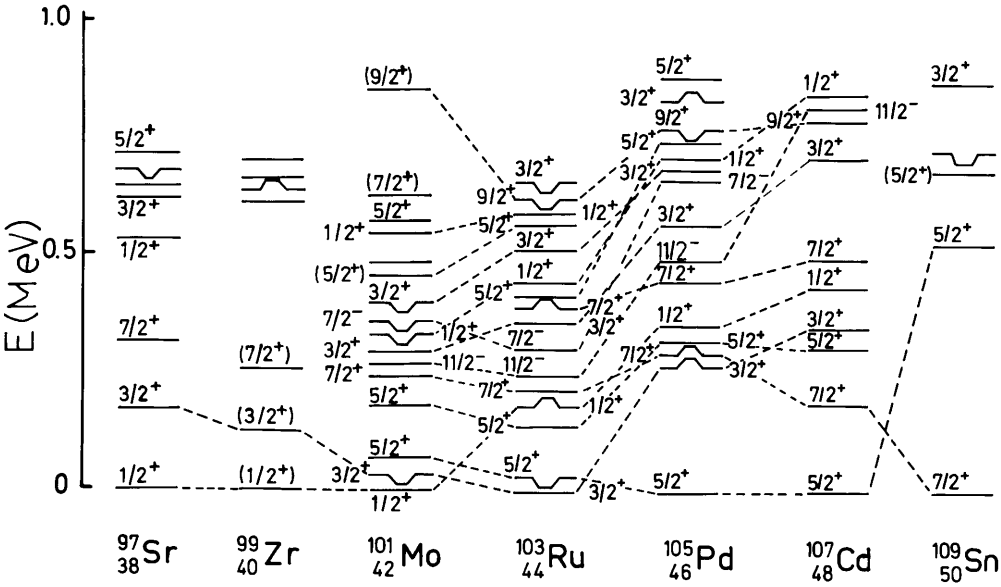

FIG. 7. Systematics of the experimentally known low-energy levels of the odd-mass $N=59$ isotones.

the ^{102}Ru nucleus) is rather similar to the boson core for ^{105}Pd (i.e., the ^{104}Pd nucleus). In both cases the core exhibits a perturbed U(5) character. Thus, the sudden change of pattern going from ^{105}Pd to ^{103}Ru is not consistent with similarity of the corresponding core nuclei. However, such a change of pattern can be achieved in the IBFM as a consequence of the change in boson-fermion interaction strengths. The IBFM calculation for ^{103}Ru [40] gives the wave functions of the low-lying states which in its boson structure differ sizably from those for ^{105}Pd, although the IBM boson core is similar in both cases. Namely, while the largest components in the wave functions of low-lying states of ^{105}Pd contain zero or one d boson, for ^{103}Ru the components are rather scattered, the largest containing about five d bosons. This means that in ^{103}Ru the boson-fermion interaction has generated an effective boson core which differs from the one which corresponds to the IBM core parameters used as input in the IBFM calculation. This means that the boson-fermion interaction polarizes the core in the odd-even system, inducing an effective deformation. Namely, we note that the IBM wave function associated with U(3) limiting symmetry exhibits a spreading of the wave function over components with different numbers of d bosons, the largest amplitude having about $n_d \approx \frac{2}{3}N$ d bosons [32], which is in our case $\frac{2}{3} \times 7 \approx 4$. Concluding, in ^{103}Ru the boson-fermion interaction destroys the quasiweak-coupling pattern which appears for ^{105}Pd, and polarizes the core; thus it generates a new pattern which bears some characteristics of the pattern associated with the U(3) boson core.

One might argue whether this change in the boson-fermion interaction between ^{105}Pd and ^{103}Ru might be associated with a change in the total strength of the proton-neutron interaction between the $1g_{9/2}$ proton and $1g_{7/2}$ neutron spin-orbit partners. That is, in zeroth order, the $Z=46$, $N=59$ isotone ^{105}Pd has a more than half-filled $1g_{9/2}$ proton configuration (six) while ^{103}Ru has a less than half-filled $1g_{9/2}$ proton configuration (four). We note that, previously, a possible role of the spin-orbit partners in this mass region has been pointed out by Federman and Pittel [44].

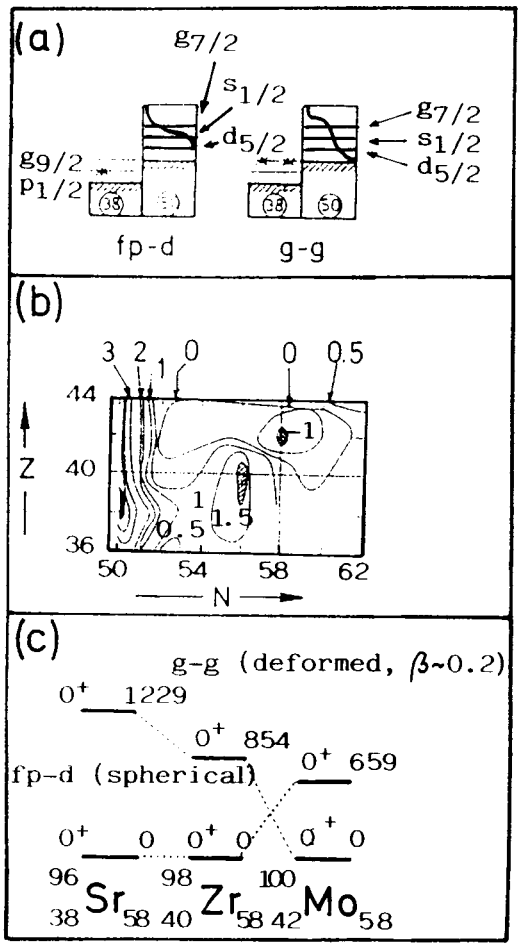

FIG. 8. (a) Conceptual structure of spherical (left) and ''deformed'' (right) structures, (b) contour plot of four-particle four-hole (4p4h) excitation energies in the mass-100 region (note the negative energy at $Z=42$ and $N=58$, i.e. ^{100}Mo), and (c) the 0^+ states that have been identified as the sperical (proton $f_{7/2}$,$p_{1/2}$, neutron $d_{5/2}$) and 4p4h (proton $g_{9/2}$, neutron $g_{7/2}$) structures in the $N=58$ isotones. Note the inversion of structures between ^{98}Zr$_{58}$ and ^{100}Mo$_{58}$ which are the core nuclei for ^{99}Zr$_{59}$ and ^{101}Mo$_{59}$, respectively (see text and Ref. [52] for details).

The next lighter isotone in the $N=59$ sequence is ^{101}Mo. The low-energy structure of this nucleus has become experimentally clarified by using transfer studies of Habib and co-workers [45], in combination with the previous beta-decay and neutron-capture gamma-ray studies [46]. Overall the levels of ^{101}Mo show a marked resemblence to the level structure of ^{103}Ru. Such should, on the surface, be expected since the associated core nuclei exhibit a similar character, i.e., between SU(5) and O(6). The IBFM calculation [47] which uses such a core has reproduced the observed levels. Although a more detailed comparison must await a more extensive knowledge of the deexciting transitions, the present calculations do correctly predict the experimentally known level lifetimes, spectroscopic factors, and deexcitation patterns of the 14- and 57-keV levels. This has not been possible in earlier attempts [1].

As seen in Fig. 7, there is a sharp difference in the level spectra for the $Z>40$, $N=59$ isotones compared with the $Z\leqslant 40$, $N=59$ isotones [48–54]. Although [53] the $1/2_1^+$ and $3/2_1^+$, ground state (g.s.) and first excited state, remain in ^{97}Sr and ^{99}Zr, there is a sharp change in the level spectra compared with the $Z>40$ isotones. However, this is expected as a consequence of dual double-subshell closure in the ^{96}Zr and ^{98}Zr pair and an extensive set of coexisting collective excitations (nine levels) in ^{98}Zr [52]. As shown in Fig. 8(a), the mechanism involves promotion of $1g_{9/2}$ protons (p) and the mutual polarization of $1g_{7/2}$ neutrons (n) which leads to the contour plot of $1g_{9/2}$-p, $1g_{7/2}$-n four-particle–four-hole (4p4h) excitations presented in Fig. 8(b). (For detailed explanation see Ref. [52].) Figure 8(c) shows the experimental verification that the predicted inversion of g.s. character occurs between ^{98}Zr and ^{100}Mo (see Ref. [52] for details). Thus, the distinct change in level spectra character below ^{101}Mo is consistent with the change in the core g.s. character. However, a quantitative accounting must await more precise information on the level characteristics of these $N=59$ isotones with $Z<42$. Also, some evidence that there may be states built on the known 4p4h coexisting states in ^{96}Sr and ^{98}Zr is given [48,54] by the observation of nanonsecond isomers in both ^{97}Sr and ^{99}Zr.

ACKNOWLEDGMENTS

Three of us (R.A.M., S.B., and V.P.) would like to express our appreciation to O.W.B. Schult for his hospitality and encouragement during our residence at Institut für Kernphysik as well as Dr. K. Sistemich and members of the JOSEPH group for the numerous discussions and sharing of information prior to publication. This work was supported, in part, under the auspices of the U.S. Department of Energy by Lawrence Livermore National Laboratory under Contract No. W-7405-Eng-48.8.

[1] R.A. Meyer, Hyperfine Interac. **22**, 385 (1985).
[2] R.A. Meyer and V. Paar, *Nuclear Structure, Reactions, and Symmetries* (World Scientific, Singapore, 1986).
[3] R.A. Meyer and V. Paar, *Symmetries and Nuclear Structure* (Hardwood Academic Press, New York, 1987).
[4] H.A. Smith, Jr. and F.A. Rickey, Phys. Rev. C **14**, 1946 (1974).
[5] R. Popli, F.A. Rickey, and P.C. Simms, Phys. Rev. C **22**, 1121 (1980).
[6] Y.A. Ellis, Nucl. Data **27**, 1 (1979).
[7] T. Suter, P. Reyes-Suter, W. Scheuer, A. Asa, and G. Backstrom, Ark. Phys. **20**, 421 (1961).
[8] H. Kawakami and H. Hisatake, Nucl. Phys. **A149**, 523 (1970).
[9] R.B. Begzhanov, A.I. Muminov, Y.Y. Radzhonov, and U.Y. Yuldashev, in Proceedings of the 21st Annual Conference on Nuclear Structure, Moscow, 1971 (unpublished).
[10] M. Behar and Z.W. Grabowski, Nucl. Phys. **A196**, 412 (1972).
[11] J. Rivier and A. Gizon, Acad. Sci. B **226**, 1161 (1968).
[12] D. Vermeulen, K. Farzine, and H.V. Buttlar, Z. Phys. A **285**, 329 (1978).
[13] K. Krien, E.H. Spejewski, R.A. Naumann, and H. Hubel, Phys. Rev. C **6**, 1847 (1972).
[14] V.D. Abukhov, M.A. Al-Amili, M.R. Akhmed, K.A. Baskova, S.S. Vasil'ev, L.I. Govor, A.M. Demidov, S. AlNadzhar, Kh.I. Shakarchi, and T.V. Chugai, Bull. Acad. Sci. USSR Phys. Ser. **40**, 106 (1977).
[15] S.V. Jackson, Lawrence Livermore National Laboratory Report No. UCRL-51846, 1976; Ph.D. thesis, University of Maryland, 1975.
[16] R. Gunnink and J.B. Niday, LLNL Report No. UCRL-51061, 1971, Vols. I–IV.
[17] R.S. Hager and E.C. Seltzer, Nucl. Data A **4**, 1 (1968).
[18] A.H. Wapstra and G. Audi, Nucl. Phys. **A432**, 1 (1985).
[19] N.B. Gove and M.J. Martin, Nucl. Data Tables A **10**, 206 (1971).
[20] W.R. Pierson and K. Rengan, Phys. Rev. **159**, 939 (1967).
[21] R.E. Anderson, R.L. Bunting, J.D. Burch, S.R. Chinn, J. Kraushaar, R.J. Petersen, D.E. Prull, B.W. Ridley, and R.A. Risyinen, Nucl. Phys. **A242**, 75 (1975).
[22] B. Cujec, Phys. Rev. **131**, 735 (1963).
[23] E. Bodenstedt (private communication).
[24] D. De Frenne, E. Jacobs, M. Verboven, and P. De Gelder, Nucl. Data Sheets **47**, 261 (1986); D. De Frenne and E. Jacobs, *ibid.* **68**, 935 (1993).
[25] J. Blachot, Nucl. Data Sheets **45**, 701 (1985).
[26] J. Blachot, J.P. Husson, J. Oms, and G. Berrier, Nucl. Data Sheets **41**, 325 (1984).
[27] A. Arima and F. Iachello, Phys. Rev. Lett. **35**, 1069 (1975).
[28] D. Janssen, R.V. Jolos, and F. Dönau, Nucl. Phys. **A224**, 93 (1974).
[29] A. Arima and F. Iachello, Ann. Phys. (N.Y.) **99**, 253 (1976).
[30] F. Iachello and O. Scholten, Phys. Rev. Lett. **43**, 679 (1979).
[31] O. Scholten, Ph.D. thesis, University of Groningen, 1980.
[32] V. Paar, S. Brant, L.F. Canto, G. Leander, and M. Vouk, Nucl. Phys. **A378**, 41 (1982); V. Paar and S. Brant, Phys. Lett. **74B**, 297 (1978).
[33] Y. Tokunaga, H. Seyfarth, R.A. Meyer, O.W.B. Schult, H.G. Börner, G. Barreau, H.R. Faust, K. Schreckenbach, S. Brant, V. Paar, M. Vouk, and D. Vretenar, Nucl. Phys. **A430**, 269 (1984).
[34] M.A. Cunningham, Nucl. Phys. **A385**, 204 (1982).

[35] S. Brant, V. Paar, D. Vretenar, and R.A. Meyer, Phys. Rev. C **34**, 342 (1986).
[36] A. Marinov, W. Oelert, S. Gopal, B. Brinkmöller, G. Hlawatsch, C. Mayer-Böricke, J. Meissburger, D. Paul, M. Rogge, J.G.M. Römer, J.L. Tain, P. Turek, L. Zemlo, R.B.M. Mooy, P.W.M. Glaudemans, S. Brant, V. Paar, M. Vouk, and V. Lopac, Nucl. Phys. **A438**, 429 (1985); A. Marinov, G.P.A. Berg, J. Bojowald, S. Gopal, S. Hürilimann, I. Katayama, S.A. Martin, C. Mayer-Böricke, J. Meissburger, W. Oelert, J.G.M. Römer, M. Rogge, J.L. Tain, P. Turek, L. Zemlo, R.B.M. Mooy, P.W.M. Glaudemans, S. Brant, V. Paar, M. Vouk, and V. Lopac, *ibid.* **A431**, 317 (1984).
[37] S. Brant and V. Paar, Phys. Lett. **143B**, 1 (1984).
[38] A. Bockisch, M. Miller, A.M. Kleinfeld, A. Gelberg, and U. Kaup, Z. Phys. A **292**, 265 (1979).
[39] Y. Tokunaga, H. Seyfarth, R.A. Meyer, O.W.B. Schult, H.G. Börner, G. Barreau, H.R. Faust, K. Schreckenbach, S. Brant, V. Paar, M. Vouk, and D. Vretenar, Nucl. Phys. **A439**, 427 (1985).
[40] H. Seyfarth, K. Schreckenbach, R.A. Meyer, S. Brant, N. Kaffrell, and V. Paar (unpublished).
[41] W. Andrejtscheff, K.D. Schilling, and P. Manfrass, At. Data Nucl. Data Tables **16**, 515 (1975).
[42] A. Bohr and B.R. Mottelson, *Nuclear Structure* (Benjamin, New York, 1975), Vol. II.
[43] V. Paar, Nucl. Phys. **A211**, 29 (1973).
[44] P. Federman and S. Pittel, Phys. Lett. **69B**, 385 (1977).
[45] E.E. Habib, J.A. Cameron, G.U. Din, V.P. Jansen, and R. Schubank, McMaster University Accelerator Laboratory 1984 Annual Report, 1984, p. 48; and (private communication).
[46] H. Ahrens, N. Kaffrel, N. Trautmann, and G. Herrmann, Phys. Rev. C **14**, 211 (1976).
[47] H. Seyfarth, H.H. Güven, B. Kardon, W.D. Lauppe, G. Lhersonneau, K. Sistemich, S. Brant, N. Kaffrell, P. Maier-Komor, H.K. Vonach, V. Paar, D. Vorkapić, and R.A. Meyer, Z. Phys. A **339**, 269 (1991).
[48] H. Selic, G. Sadler, T.A. Khan, W.D. Lauppe, H. Lawin, K. Sistemich, E. Monnand, J. Blachot, and F. Schussler, Z. Phys. A **289**, 197 (1979).
[49] R.A. Meyer, E. Monnand, J.A. Pinston, F. Schussler, I. Ragnarsson, B. Pfeiffer, H. Lawin, G. Lhersonneau, T. Seo, and K. Sistemich, Nucl. Phys. **A439**, 510 (1985).
[50] K.-L. Kratz, H. Ohm, A. Schröder, H. Gabelmann, W. Ziegert, B. Pfeiffer, G. Jung, E. Monnand, J.A. Pinston, F. Schussler, G.I. Crawford, S.G. Prussin, and Z.M. de Oliveira, Z. Phys. A **312**, 43 (1983).
[51] K. Heyde, P. van Isacker, M. Waroquer, J.L. Wood, and R.A. Meyer, Phys. Rep. **102**, 291 (1983).
[52] R.A. Meyer, E.A. Henry, L.G. Mann, and K. Heyde, Phys. Lett. B **177**, 271 (1986).
[53] F. Buchinger, E.B. Ramsay, R.E. Silverans, P. Lievens, E. Arnold, W. Neu, R. Neugart, G. Ulm, K. Wendt, and the ISOLDE Collaboration, Z. Phys. A **327**, 361 (1987); R. Neugart (private communication).
[54] K. Kawade, G. Lhersonneau, H. Ohm, K. Sistemich, and R.A. Meyer, 1986 Annual Report, IKP-KFA Jülich, Germany, 1987.